JACS
JOURNAL OF THE AMERICAN CHEMICAL SOCIETY
Article
pubs.acs.org/JACS

Mononuclear Nonheme High-Spin Iron(III)-Acylperoxo Complexes in Olefin Epoxidation and Alkane Hydroxylation Reactions

Bin Wang,[†] Yong-Min Lee,[†] Martin Clémancey,[‡] Mi Sook Seo,[†] Ritimukta Sarangi,*[,¶] Jean-Marc Latour,*[,‡] and Wonwoo Nam*[,†]

[†]Department of Chemistry and Nano Science, Ewha Womans University, Seoul 03760, Korea

[‡]University of Grenoble Alpes, LCBM/PMB and CEA, IRTSV/CBM/PMB and CNRS, LCBM UMR 5249, PMB, 38000 Grenoble, France

[¶]Stanford Synchrotron Radiation Lightsource, SLAC National Accelerator Laboratory, Stanford University, Menlo Park, California 94025-7015, United States

Supporting Information

ABSTRACT: Mononuclear nonheme high-spin iron(III)-acylperoxo complexes bearing an N-methylated cyclam ligand were synthesized, spectroscopically characterized, and investigated in olefin epoxidation and alkane hydroxylation reactions. In the epoxidation of olefins, epoxides were yielded as the major products with high stereo-, chemo-, and enantioselectivities; *cis*- and *trans*-stilbenes were oxidized to *cis*- and *trans*-stilbene oxides, respectively. In the epoxidation of cyclohexene, cyclohexene oxide was formed as the major product with a kinetic isotope effect (KIE) value of 1.0, indicating that nonheme iron(III)-acylperoxo complexes prefer C═C epoxidation to allylic C−H bond activation. Olefin epoxidation by chiral iron(III)-acylperoxo complexes afforded epoxides with high enantioselectivity, suggesting that iron(III)-acylperoxo species, not high-valent iron-oxo species, are the epoxidizing agent. In alkane hydroxylation reactions, iron(III)-acylperoxo complexes hydroxylated C−H bonds as strong as those in cyclohexane at −40 °C, wherein (a) alcohols were yielded as the major products with high regio- and stereoselectivities, (b) activation of C−H bonds by the iron(III)-acylperoxo species was the rate-determining step with a large KIE value and good correlation between reaction rates and bond dissociation energies of alkanes, and (c) the oxygen atom in the alcohol product was from the iron(III)-acylperoxo species, not from molecular oxygen. In isotopically labeled water ($H_2{}^{18}O$) experiments, incorporation of ^{18}O from $H_2{}^{18}O$ into oxygenated products was not observed in the epoxidation and hydroxylation reactions. On the basis of mechanistic studies, we conclude that mononuclear nonheme high-spin iron(III)-acylperoxo complexes are strong oxidants capable of oxygenating hydrocarbons prior to their conversion into iron-oxo species via O−O bond cleavage.

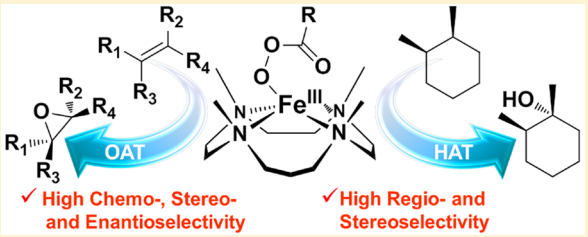

INTRODUCTION

Metal-oxygen intermediates that are involved in the catalytic oxidation of organic substrates by O_2-activating metalloenzymes and their model compounds have been investigated intensively over several decades in heme systems and more recently in mononuclear nonheme iron systems.[1−3] In cytochromes P450 (P450) and iron porphyrin models, high-valent iron(IV)-oxo porphyrin π-cation radicals, referred to as compound I (Cpd I), have been widely accepted as reactive intermediates in the catalytic oxygenation reactions.[2] Indeed, Cpd I has been captured, spectroscopically characterized, and investigated in reactivity studies in P450.[4] In iron porphyrin models, the reactivity and mechanistic studies of synthetic Cpd I complexes have shown that Cpd I is a highly reactive and powerful oxidant in various oxidation reactions, including olefin epoxidation and alkane hydroxylation.[2]

The high-valent iron(IV)-oxo intermediates have also been identified and characterized spectroscopically and/or structurally in mononuclear nonheme iron enzymes and synthetic nonheme iron complexes.[3] The reactivities of the nonheme iron-oxo species have been well investigated recently in various oxidation reactions, including the oxidation of olefins and the C−H bond activation reactions, with synthetic iron(IV)-oxo complexes under stoichiometric conditions.[2b,3,5] For example, factors affecting reactivities and reaction mechanisms of the nonheme iron(IV)-oxo complexes, such as the structural and electronic effects of supporting and axial ligands, the spin states of iron(IV) ion, and the binding of proton and redox-inactive metal ions, have been well addressed in the reactivity studies.[3,5] Thus, the chemistry of the nonheme iron-oxo intermediates has been advanced greatly since the first two reports on the enzymatic and biomimetic studies appeared in 2003.[6]

In addition to the high-valent iron-oxo species, other iron-oxygen intermediates, such as iron(III)-superoxo, -peroxo, and -hydroperoxo species, have been considered as active oxidants

Received: December 28, 2015
Published: January 27, 2016

DOI: 10.1021/jacs.5b13500
J. Am. Chem. Soc. 2016, 138, 2426−2436

in both heme and nonheme iron systems.[1d,7] For example, iron(III)-hydroperoxo species have been invoked as "second-electrophilic oxidants" in the catalytic oxidation of organic substrates by P450.[7] However, experimental/theoretical mechanistic studies revealed that the iron(III)-hydroperoxo species is a sluggish oxidant in heme systems.[8] The multiple oxidants hypothesis has been debated intensively in nonheme iron systems as well. One example is the reactivity of activated bleomycin (i.e., a low-spin iron(III)-OOH species), which is the last detectable intermediate in the reaction cycle of bleomycin and has been proposed as a plausible oxidant responsible for DNA cleavage.[3d,9] In biomimetic studies, a mononuclear nonheme high-spin iron(III)-hydroperoxo complex, $[(14\text{-TMC})Fe^{III}(OOH)]^{2+}$ (14-TMC = 1,4,8,11-tetramethyl-1,4,8,11-tetraazacyclotetradecane), was recently shown to be a competent oxidant in both electrophilic and nucleophilic oxidative reactions;[10] the spin state of iron(III)-hydroperoxo species is an important factor that determines their oxidizing power.[11]

Other metal-oxidant adducts (M^{n+}-OX, X = IAr, OC(O)R, and halides) have been synthesized and characterized spectroscopically and/or structurally in biomimetic studies.[12−14] These isolated and/or in situ generated metal-oxidant adducts were then examined in various oxidation reactions, such as in oxygen atom transfer (OAT) and hydrogen atom transfer (HAT) reactions. In most cases, metal-oxidant adducts showed moderate reactivities, implying that the metal-oxidant adducts are competent oxidants but are much less reactive than their corresponding high-valent metal-oxo complexes.[12] However, it has been shown very recently that mononuclear nonheme high-spin iron(III)-iodosylarene adducts bearing an N-methylated cyclam ligand, $[(13\text{-TMC})Fe^{III}\text{-OIAr}]^{3+}$ (13-TMC = 1,4,7,10-tetramethyl-1,4,7,10-tetraazacyclotridecane), are highly reactive in both OAT and HAT reactions, even more reactive than the iron(IV)-oxo complex bearing the same supporting ligand, $[(13\text{-TMC})Fe^{IV}(O)]^{2+}$.[13]

Among the metal-oxidant adducts, metal-acylperoxo complexes, M^{n+}-OOC(O)R, have been frequently used in investigating the nature of the O−O bond activation to form high-valent metal-oxo species (e.g., heterolytic versus homolytic O−O bond cleavage).[14] Although the mechanistic studies provided valuable information on the elucidation of the O−O bond cleavage mechanisms, the reactivity of the metal-acylperoxo species in oxidation reactions has been less clearly understood and remains elusive. Herein, we report for the first time that mononuclear nonheme high-spin iron(III)-acylperoxo complexes bearing an N-methylated cyclam ligand are highly reactive in olefin epoxidation and alkane hydroxylation reactions (Scheme 1); epoxides and alcohols are formed as the major products with high chemo-, stereo-, regio-, and enantioselectivities. We also provide experimental evidence supporting that the iron(III)-acylperoxo complexes are active oxidants that effect the olefin epoxidation and alkane hydroxylation reactions.

Scheme 1. Mononuclear Nonheme High-Spin Iron(III)-Acylperoxo Complex in Olefin Epoxidation and Alkane Hydroxylation Reactions

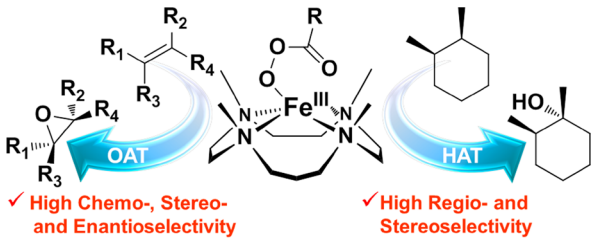

RESULTS AND DISCUSSION

Generation and Characterization of Iron(III)-Acylperoxo Complexes. Treatment of $[Fe^{II}(13\text{-TMC})(CF_3SO_3)_2]$ with 4 equiv of peroxycarboxylic acids, such as phenylperoxyacetic acid (PPAA), peroxybenzoic acid (PBA), *m*-chloroperoxybenzoic acid (*m*-CPBA), and peroxyacetic acid (PAA), in a solvent mixture of CF_3CH_2OH and acetone (v/v = 3:1) at −40 °C resulted in the formation of blue intermediates within 30 s to 2 min; the formation time changes slightly depending on the peracids used. These intermediates, denoted as **1** (from the reaction with PPAA), **2** (from the reaction with PBA), **3** (from the reaction with *m*-CPBA), and **4** (from the reaction with PAA), show a maximum UV−vis absorption band at 660 nm (Figure 1a for **1**; Supporting Information (SI), Figure S1 for **2**−**4**). These metastable intermediates ($t_{1/2}$ = ∼ 20 min at −40 °C) were characterized using various spectroscopic techniques, such as electron paramagnetic resonance (EPR) spectroscopy, coldspray ionization time-of-flight mass spectrometer (CSI-TOF MS), Mössbauer, and X-ray absorption spectroscopy (XAS). The X-band EPR spectra of **1**−**4**, recorded in a frozen CF_3CH_2OH/acetone (3:1) solution at 5 K, exhibit signals that are characteristic of $S = 5/2$ Fe^{III} (Figure 1b for **1**; SI, Figure S2 for **2**−**4**).[13,15] In addition, EPR signals corresponding to nonheme $Fe^{V}(O)$ species (e.g., *g* values at ∼2)[16] were not detected in the solutions of **1**−**4**. In the CSI-TOF MS of **1**−**4**, we detected mass peaks corresponding to the iron(III)-acylperoxo species only in a small quantity (∼3% mass height, data not shown), probably due to the instability of the intermediates under the mass spectrometer conditions. In contrast to the iron(III)-acylperoxo complexes, we reported recently strong mass peaks (e.g., ∼30% mass height) corresponding to iron(III)-iodosylarene complexes, $[(13\text{-TMC})Fe^{III}\text{-OIAr}]^{3+}$.[13]

Mössbauer spectrum of **1** recorded at 5 K in a weak magnetic field of 600 G applied parallel to the γ rays (SI, Figure S3) is dominated by two quadrupole doublets with an isomer shift close to zero, which suggests the presence of iron(IV) species. In addition, a diffuse absorption is spread over a large velocity domain (from −6 to +6 mm s^{-1}). Application of a magnetic field from 1 to 7 T, applied parallel to the γ rays, allowed us to confirm that the doublets correspond to $S = 1$ species, whose parameters match those of classical iron(IV)-oxo complexes.[17] In addition, the magnetic field turned the broad absorption into a sextet. The series of all four spectra were simulated within the spin Hamiltonian formalism and the sextet assigned to an $S = 5/2$ species accounting for approximately 36% of the total iron (Figure 1c; SI, Table S1 for complete parameters).[18] Accordingly, **1** is assigned as a high-spin iron(III) species, which degrades into two iron(IV)-oxo products (vide infra).

Fe K-edge XAS was performed on solutions of $[Fe^{II}(13\text{-TMC})(CF_3SO_3)_2]$ and **1**, and the data are presented in Figure 2a. XAS data for $[(13\text{-TMC})Fe^{IV}(O)]^{2+}$ are included for comparison,[19] which shows that **1** is clearly shifted to higher energy relative to $[Fe^{II}(13\text{-TMC})(CF_3SO_3)_2]$, which is consistent with the oxidation of the starting Fe(II) complex. A comparison of the pre-edge region of **1** with $[(13\text{-TMC})Fe^{IV}(O)]^{2+}$ shows a pre-edge feature that is significantly

DOI: 10.1021/jacs.5b13500
J. Am. Chem. Soc. 2016, 138, 2426−2436

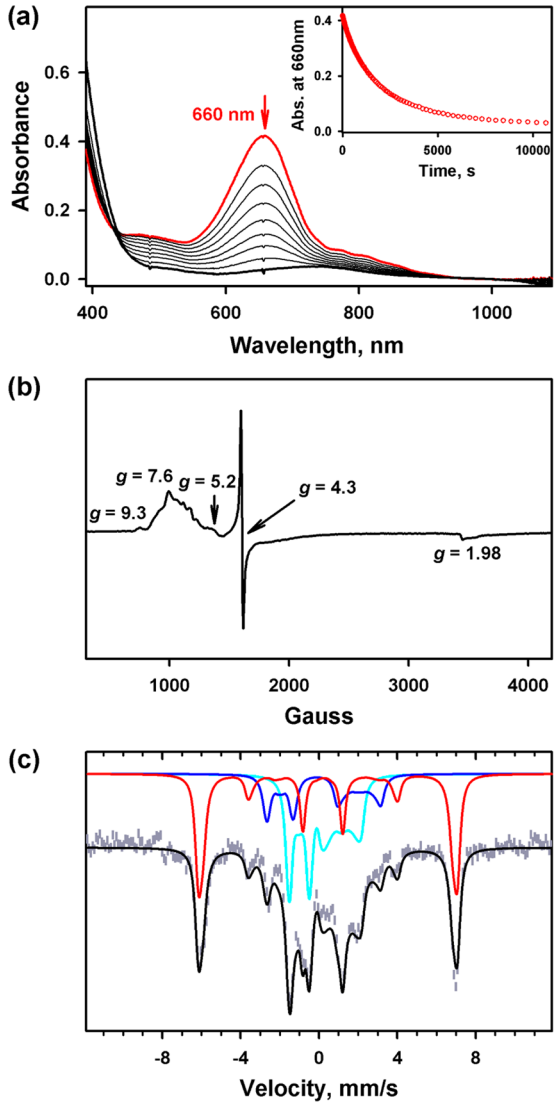

Figure 1. (a) UV−vis spectral changes for the natural decay of **1**, which was generated within 30 s with a maximum absorption band at λ = 660 nm in the reaction of $[Fe^{II}(13\text{-TMC})(CF_3SO_3)_2]$ (1.0 mM) and PPAA (4 equiv) in CF_3CH_2OH/acetone (3:1) at −40 °C. The inset shows the time course monitored at 660 nm for the natural decay of **1**. (b) X-band EPR spectrum of **1** (1.0 mM). (c) Mössbauer spectra of **1** recorded at 4.2 K in a magnetic field of 7 T applied parallel to the γ rays. The vertical gray bars are the experimental points, and the solid black line is the theoretical spectrum generated by spin Hamiltonian simulations. Components are assigned to **1** (red) and two Fe^{IV} products (blue and cyan).

more intense and lower in energy by ∼0.4 eV, indicating the presence of a highly distorted Fe(III) site. To confirm this, EXAFS data were measured on **1**, and the best fits are shown in Figure 2b. The data are consistent with a first shell with 0.5 Fe−O at 1.66 Å and 0.5 Fe−O at 1.92 Å. The second shell is fit with 4 Fe−N components at 2.12 Å (see SI, Table S2 for complete fits). The σ^2 values for all first-shell parameters are somewhat higher, indicating that the species is a ∼1:1 mixture of **1** and the $[(13\text{-TMC})Fe^{IV}(O)]^{2+}$ forms. This is also indicated by the presence of the 0.5 short Fe−O component. The pre-edge and EXAFS data indicate that **1** is a highly distorted Fe(III) species with an Fe−O distance of ∼1.92 Å. It is likely that a weak Fe···O═C coordination also exists, distorting the site but is not observed from the EXAFS analysis.

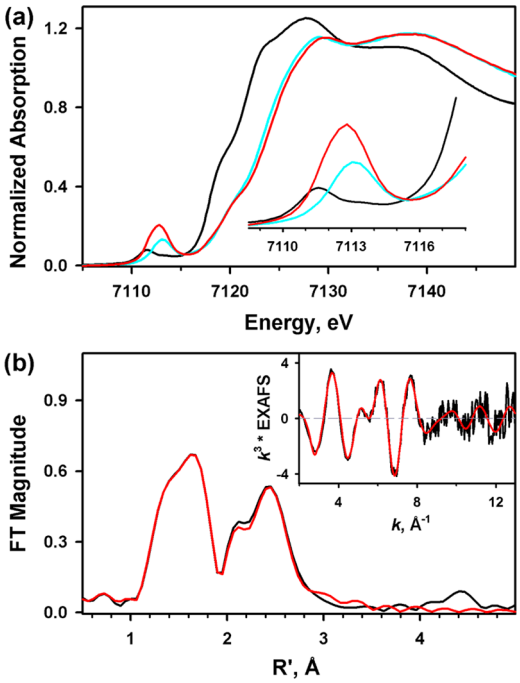

Figure 2. (a) The normalized Fe K-edge XAS data for $[Fe^{II}(13\text{-TMC})(CF_3SO_3)_2]$ (black), **1** (red), and $[(13\text{-TMC})Fe^{IV}(O)]^{2+}$ (cyan). The inset shows the expanded pre-edge region. (b) Nonphase-shift corrected Fourier transform (FT) data (black line) and the corresponding FEFF fit (red line) to the Fe K-edge FT data for **1**. The inset shows the EXAFS data (black line) and fit (red line).

Based on the spectroscopic characterization presented above, we are able to propose the formation of mononuclear nonheme high-spin iron(III)-acylperoxo complexes in the reactions of $[Fe^{II}(13\text{-TMC})(CF_3SO_3)_2]$ with peroxycarboxylic acids, such as $[(13\text{-TMC})Fe^{III}(OOC(O)CH_2Ph)]^{2+}$ (**1**), $[(13\text{-TMC})Fe^{III}(OOC(O)Ph)]^{2+}$ (**2**), $[(13\text{-TMC})Fe^{III}(OOC(O)C_6H_4Cl)]^{2+}$ (**3**), and $[(13\text{-TMC})Fe^{III}(OOC(O)CH_3)]^{2+}$ (**4**).

Epoxidation of Olefins by Iron(III)-Acylperoxo Complexes (1−4). Reactivities of the nonheme iron(III)-acylperoxo complexes (**1**−**4**) were investigated in olefin epoxidation reactions. Addition of styrene to the solutions of **1**−**4** in a solvent mixture of CF_3CH_2OH and acetone (v/v = 3:1) at −60 °C resulted in the disappearance of the intermediates with a first-order decay profile (Figure 3a for the reaction of **1**; SI, Figure S4 for the reactions of **2**−**4**). The first-order rate constants, determined by pseudo-first-order fitting of the kinetic data for the decay of the iron(III)-acylperoxo species, increased linearly with the increase of the styrene concentration (Figure 3b for the reaction of **1**; SI, Figure S5 for the reactions of **2**−**4**), affording second-order rate constants for the reactions of **1**−**4** (SI, Table S3). A kinetic isotope effect (KIE) value of 1.0(1) was obtained in the oxidation of styrene and styrene-d_8 by **1**−**4** (Figure 3b for the reaction of **1**; SI, Figure S5 for the reactions of **2**−**4**), indicating that the oxidation of styrene by the iron(III)-acylperoxo complexes occurs by an OAT mechanism. The olefin epoxidation by **1** was also investigated with *para*-X-substituted styrenes (X = Me, H, Cl, and NO_2) and *meta*-chloro-styrene (SI, Table S4 and Figure S6). When logarithms of the second-order rate constants, log k_2, were plotted against the oxidation potentials (E_{ox}) of substrates, a good linear correlation was observed with a slope of −1.1 (Figure 3c, left panel).[13b,20] In

DOI: 10.1021/jacs.5b13500
J. Am. Chem. Soc. 2016, 138, 2426−2436

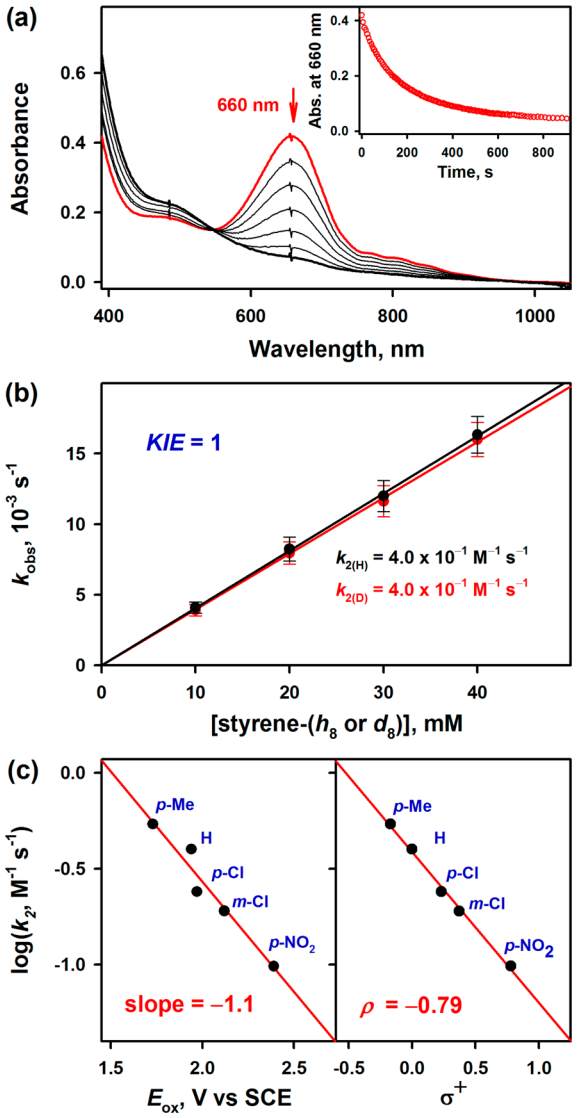

Figure 3. (a) UV–vis spectral changes observed in the reaction of **1** (1.0 mM) and styrene (10 mM) in CF_3CH_2OH/acetone (3:1) at −60 °C. The inset shows the time course monitored at 660 nm. (b) Plots of pseudo-first-order rate constants (k_{obs}) against the concentrations of styrene-h_8 (black circles) and styrene-d_8 (red circles) to determine second-order rate constants (k_2) for the oxidation of styrenes by **1** in CF_3CH_2OH/acetone (3:1) at −60 °C. (c) Plots of log k_2 against the E_{ox} values (left panel) and Hammett parameters, σ^+, (right panel) of styrene derivatives for the reactions of **1** with styrene derivatives.

addition, a ρ value of −0.79 was obtained from the Hammett plot of log k_2 against σ^+ (Figure 3c, right panel). These results indicate that the iron(III)-acylperoxo species possess electrophilic character in olefin epoxidation reactions, as observed in heme and nonheme iron(IV or V)-oxo complexes and nonheme iron(III)-iodosylarene adducts.[13b,20,21]

Product analysis of the reaction solution of the styrene epoxidation by iron(III)-acylperoxo complexes revealed the formation of styrene oxide as the major product along with a small amount of 2-phenylacetaldehyde (SI, Table S3). Similarly, the epoxidation of styrene derivatives by **1** afforded epoxide products predominantly (SI, Table S5). We also analyzed products derived from the decay of PPAA in the epoxidation of styrene by **1**, since PPAA has been frequently used as an oxidant probe in proposing O–O bond cleavage mechanisms in metal-catalyzed oxidation reactions by peroxyacids (e.g., O–O bond heterolysis versus homolysis) (Scheme 2, pathways *a* and *b*).[22] The product analysis revealed that phenylacetic acid was the major product (83(5)% yield based on the amount of PPAA used) with the formation of small amounts of toluene (1.3(5)%), benzyl alcohol (3.3(4)%), and benzaldehyde (5.4(5)%). The observation of the phenylacetic acid formation as the major product clearly indicates that the epoxidation reaction by **1** occurs via the pathways *a* or *c* in Scheme 2 (vide infra), not via the pathway *b*. In the latter case, products should derive from the initial decarboxylation of a carboalkoxy radical, such as toluene, benzyl alcohol, and benzaldehyde (see Scheme 2, pathway *b*). Finally, we found that iron(III) species was formed as the decayed product of **1** in the styrene epoxidation reaction (SI, Figure S7).

Scheme 2. Proposed Mechanisms from the Product Analysis of PPAA

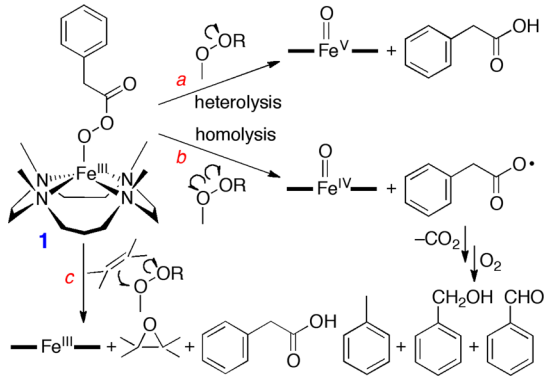

In the epoxidation of *cis*- and *trans*-stilbenes by **1**, *cis*- and *trans*-stilbene oxides were formed as the major products, respectively, with the formation of trace amounts of isomerized products (SI, Table S5, entries 5 and 6), demonstrating that the epoxidation reaction by **1** is highly stereoselective (Scheme 3 A and B). Second-order rate constants of 7.2×10^{-1} and 1.7 M^{-1} s^{-1} were also determined in the epoxidation of *cis*- and *trans*-stilbenes by **1**, respectively (SI, Table S4 and Figure S6). In addition, when **1** was reacted with equal amounts of *cis*- and

Scheme 3. Epoxidation of *cis*-Stilbene (A), *trans*-Stilbene (B), and Cyclohexene (C) by an Iron(III)-Acylperoxo Complex

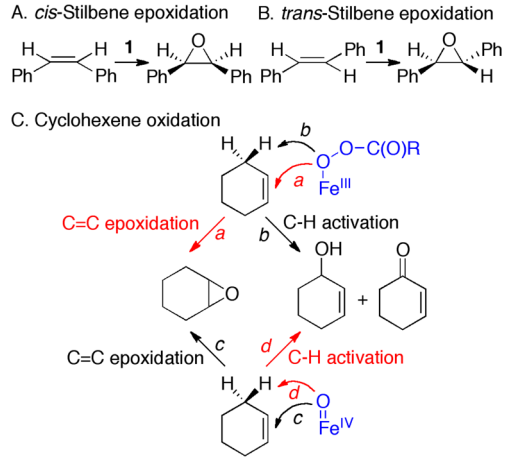

DOI: 10.1021/jacs.5b13500
J. Am. Chem. Soc. 2016, 138, 2426–2436

trans-stilbenes, the product ratio of *cis*- to *trans*-stilbene oxide was determined to be 0.32 (SI, Table S5, entry 7). The results of the kinetic studies and the competitive reaction lead us to conclude that **1** reacts faster with *trans*-stilbene than with *cis*-stilbene, probably due to the difference in the oxidation potentials of the substrates (SI, Table S4).[13b]

In the epoxidation of cyclohexene by **1**, a second-order rate constant of 7.3×10^{-1} M^{-1} s^{-1} was determined (SI, Table S6 and Figures S8 and S9). Interestingly, cyclohexene oxide was formed as the major product with small amounts of allylic oxidation products, such as cyclohexenol and cyclohexenone (SI, Table S6). This result indicates that C=C epoxidation is the predominant reaction (Scheme 3C, pathway *a*), which is different from the result of the cyclohexene oxidation by nonheme metal(IV)-oxo complexes (e.g., nonheme iron(IV)-oxo complex).[5e,23,24] In the latter reactions, cyclohexenol, derived from the C−H bond activation (Scheme 3C, pathway *d*), was the major product. In addition, while large KIE values (e.g., KIE of >30) were observed in the oxidation of cyclohexene and cyclohexene-d_{10} by nonheme metal(IV)-oxo complexes,[23,24] a KIE value of 1.0 was determined in the oxidation of cyclohexene and cyclohexene-d_{10} by iron(III)-acylperoxo complexes, **1**−**4** (SI, Figure S9); the KIE value of 1.0 supports that the oxidation of cyclohexene by the nonheme iron(III)-acylperoxo complexes occurs via the C=C epoxidation pathway (Scheme 3C, pathway *a*). Thus, based on the results of the product analysis and KIE studies, we conclude that the oxidation of cyclohexene by nonheme iron(III)-acylperoxo complexes occurs via the C=C epoxidation pathway predominantly (Scheme 3C, pathway *a*), which is different from the preference of the allylic C−H bond activation of cyclohexene by nonheme metal-oxo complexes (Scheme 3C, pathway *d*).[23,24]

We also performed the olefin epoxidation with chiral iron(III)-acylperoxo complexes, with an assumption that if the iron(III)-acylperoxo species is the epoxidizing intermediate, we would observe the formation of epoxide with an enantiomeric excess (ee) (Scheme 4A, pathway *a*). If an iron(IV or V)-oxo species is formed via O−O bond cleavage of the iron-acylperoxo complex and the resulting iron-oxo species is involved in the olefin epoxidation, only a racemic mixture would be formed (Scheme 4A, pathways *b* and *c*). We therefore prepared a pair of optically active peroxycarboxylic acids possessing a chiral center, (*R*)-2-phenylperoxypropionic acid and (*S*)-2-phenylperoxypropionic acid,[25] and used them in the synthesis of chiral iron(III)-acylperoxo complexes bearing the 13-TMC ligand, such as mononuclear nonheme high-spin $[(13\text{-TMC})Fe^{III}(OOC(O)^{R}CH(CH_3)Ph)]^{2+}$ (**5**) and $[(13\text{-TMC})Fe^{III}(OOC(O)^{S}CH(CH_3)Ph)]^{2+}$ (**6**) complexes (see Experimental Section for reaction procedures; also see SI, Figures S2 and S10 for EPR and UV−vis spectra of **5** and **6**). Interestingly, when the chiral iron(III)-acylperoxo complexes were reacted with chalcone, chalcone oxide was formed as a major product with a good enantioselectivity (Scheme 4B) (see Experimental Section for product analysis; see also SI, Figure S11 for HPLC spectra). When the epoxidation of chalcone by the peroxyacid was carried out in the absence of the iron catalyst, the formation of chalcone oxide was negligible. This control reaction demonstrated that the chalcone oxide was the epoxidation product of chalcone by the chiral iron(III)-acylperoxo complexes, not by the peroxycarboxylic acids remained in solutions. Moreover, the present results demonstrate unambiguously that the intermediate responsible for the

Scheme 4. Asymmetric Epoxidation by Chiral Iron(III)-Acylperoxo Complexes

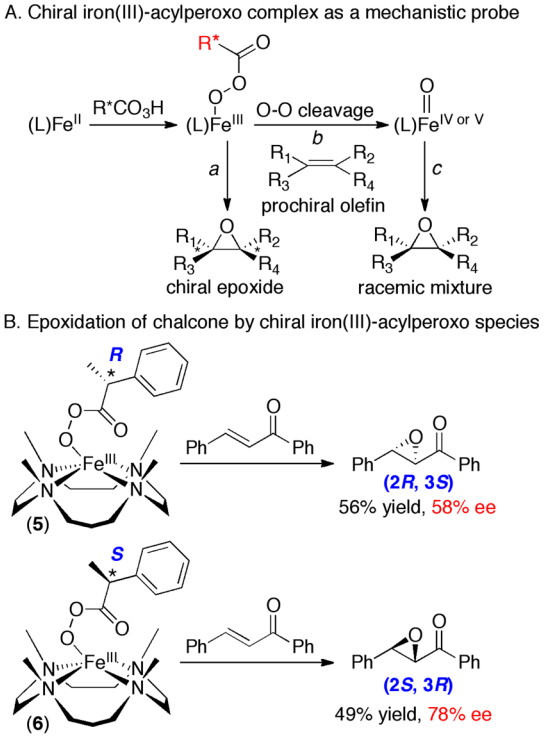

epoxidation of olefins by the iron(III)-acylperoxo species should contain a chiral center (i.e., **5** and **6**) (Scheme 4A, pathway *a*) and that the iron(IV or V)-oxo complexes formed via O−O bond cleavage, which do not possess a chiral center, are not the active oxidant for the olefin epoxidation (Scheme 4A, pathways *b* and *c*). Further, when the catalytic olefin epoxidation was performed using the optically active peroxycarboxylic acids in the presence of $[Fe^{II}(13\text{-TMC})]^{2+}$, epoxides were produced predominantly with virtually the same ee values as obtained in the stoichiometric reactions (SI, Figure S11). We therefore conclude that the catalytic epoxidation of olefins by the nonheme iron complex and peroxycarboxylic acids is mediated by the iron(III)-acylperoxo species (Scheme 4A, pathway *a*), not by the iron-oxo species (Scheme 4A, pathways *b* and *c*).

As a conclusion, we have reported that the nonheme iron(III)-acylperoxo complexes epoxidize olefins efficiently with electrophilic character. Epoxides are formed as the major products with high stereo-, chemo-, and enantioselectivities; (a) the epoxidation of *cis*- and *trans*-stilbenes by the iron(III)-acylperoxo complexes affords the corresponding *cis*- and *trans*-stilbene oxides, respectively, (b) the nonheme iron(III)-acylperoxo complexes prefer the C=C epoxidation to the C−H bond activation in the oxidation of cyclohexene, and (c) the olefin epoxidation by chiral iron(III)-acylperoxo complexes yields epoxide products with a good enantioselectivity. The latter result strongly supports that the nonheme iron(III)-acylperoxo complexes epoxidize olefins prior to the conversion into the high-valent iron-oxo species (vide infra).

Alkane Hydroxylation by Iron(III)-Acylperoxo Complexes (1−4). The iron(III)-acylperoxo complexes, **1**−**4**, were investigated in the C−H bond activation of alkanes at −40 °C. Addition of cumene to the solutions of **1**−**4** in a solvent mixture of CF_3CH_2OH and acetone (v/v = 3:1) at −40 °C

DOI: 10.1021/jacs.5b13500
J. Am. Chem. Soc. 2016, 138, 2426−2436

resulted in the disappearance of the intermediates with a first-order decay profile (see Figure 4a for the reaction of **1**; SI, Figure S12 for the reactions of **2**–**4**). The first-order rate constants, determined by first-order fitting of the kinetic data for the decay of the iron(III)-acylperoxo species at 660 nm, increased proportionally to the cumene concentration (Figure 4b; SI, Figure S13), affording second-order rate constants for the reactions of **1**–**4** (see Table S7). A second-order rate constant of 6.0×10^{-1} M^{-1} s^{-1} with a KIE value of 8.0(6) was obtained for the oxidation of cumene by **1** (Figure 4b). In the same reaction using **2**–**4**, similar second-order rate constants with the KIE value of ~8 were obtained (Figure S13). Second-order rate constants were also obtained for oxidation of other substrates by **1** (SI, Table S8 and Figure S14), showing a linear correlation between the reaction rates and the C–H bond dissociation energies (BDE) of the substrates (Figure 4c).[26] The observations of the large KIE value and the linear correlation between the reaction rates and the BDEs of substrates lead us to conclude that the C–H bond activation of substrates by the iron(III)-acylperoxo species is the rate-determining step.

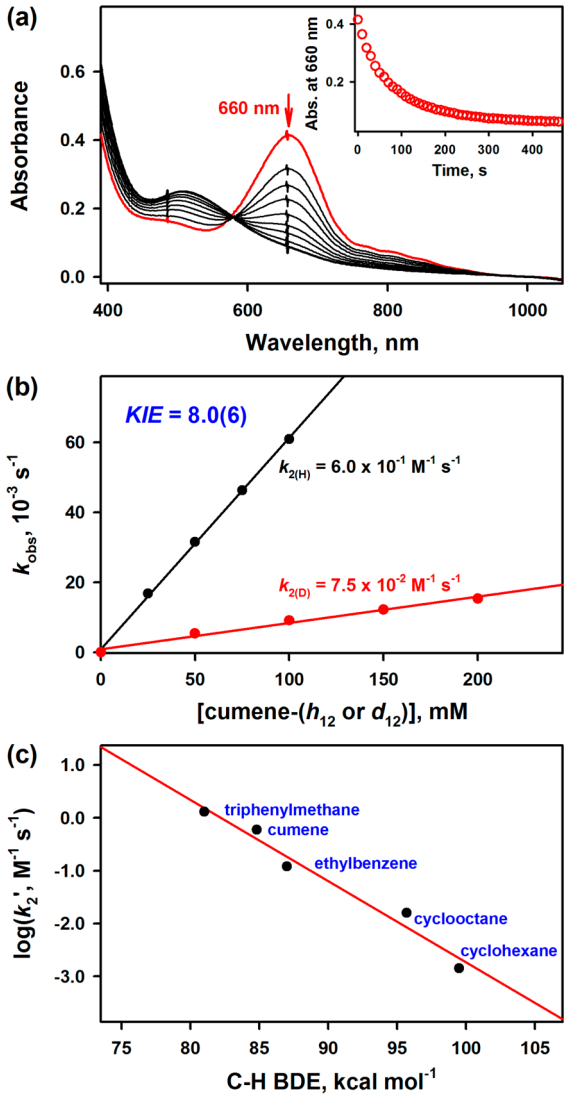

Figure 4. (a) UV–vis spectral changes observed in the reaction of **1** (1.0 mM) and cumene (25 mM) in CF_3CH_2OH/acetone (3:1) at −40 °C. Inset shows the time course monitored at 660 nm. (b) Plots of pseudo-first-order rate constants, k_{obs}, against concentrations of cumene-h_{12} (black circles) and cumene-d_{12} (red circles) to determine second-order rate constants (k_2) in CF_3CH_2OH/acetone (3:1) at −40 °C. (c) Plot of log k_2′ versus C–H BDEs of substrates. The k_2′ values are obtained by dividing second-order rate constants (k_2) by the number of equivalent target C–H bonds in the substrates.

Product analysis of the reaction solutions revealed the formation of alcohols as the major product in the oxidation of alkanes by **1**–**4** (SI, Tables S7 and S9). For example, the oxidation of cumene by **1** under an inert atmosphere produced 2-phenylpropan-2-ol (39(4)%), α-methylstyrene (13(3)%), and acetophenone (3.0(6)%). Importantly, when the cumene oxidation by **1** was carried out under $^{18}O_2$ atmosphere, the oxygen atom in the 2-phenylpropan-2-ol product contained ^{16}O derived from **1**, not ^{18}O derived from $^{18}O_2$ (Scheme 5A; SI, Figure S15). Analysis of the decayed product of **1** in the oxidation of cumene with electrospray ionization mass spectrometer (ESI-MS) and EPR showed the formation of Fe(III) species (Experimental Section and SI, Figure S16).

Scheme 5. $^{18}O_2$ Experiment and Regio- and Stereoselectivities in Hydroxylation Reactions by an Iron(III)-Acylperoxo Complex

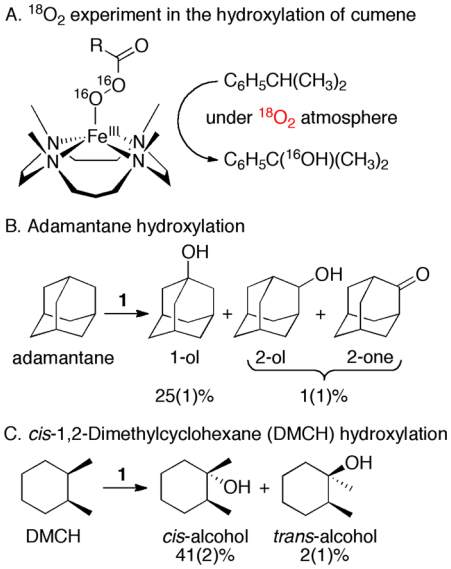

The regio- and stereoselectivities in the alkane hydroxylation reactions by iron(III)-acylperoxo complexes were investigated using substrate probes, such as adamantane and *cis*-1,2-dimethylcyclohexane (DMCH). In the hydroxylation of adamantane by **1**, a high preference for the tertiary C–H bonds (BDE of 3° C–H = 96.2 kcal mol^{-1})[26] over the secondary C–H bonds (BDE of 2° C–H = 100.2 kcal mol^{-1})[26] was observed, giving a normalized 3°/2° ratio of ~75 (Scheme 5B). This result indicates that the alkane hydroxylation by **1** is highly regioselective, as observed in other catalytic oxidation reactions by metalloporphyrin and nonheme iron complexes.[27] More importantly, hydroxylation of DMCH by **1** produced *cis*-1,2-dimethylcyclohexanol as the major product with a small amount of an isomerized alcohol product, *trans*-1,2-dimethylcyclohexanol (Scheme 5C). The latter result indicates that the hydroxylation reaction by **1** is highly stereoselective, as reported in the catalytic hydroxylation reactions by iron porphyrin and nonheme iron complexes.[28]

DOI: 10.1021/jacs.5b13500
J. Am. Chem. Soc. 2016, 138, 2426–2436

In summary, we have shown that the nonheme iron(III)-acylperoxo complexes are highly reactive species that can hydroxylate alkane C−H bonds as strong as those in cyclohexane at −40 °C; alcohols are yielded as the major products with high regio- and stereoselectivities, and the source of the oxygen atom in the alcohol product is the iron(III)-acylperoxo species, not molecular oxygen. We have also shown that the alkane hydroxylation by the iron(III)-acylperoxo species occurs via the rate-determining C−H bond activation step, with a large KIE value and a good correlation between the reaction rates and the BDEs of alkanes.

Isotopically Labeled Water Experiments. Since it is extremely difficult to identify the nature of intermediates involved in the catalytic oxygenation of organic substrates by enzymes and metal catalysts, isotopically labeled water ($H_2{}^{18}O$) experiments have been frequently used as indirect evidence for the intermediacy of high-valent metal-oxo species in the catalytic oxygenation reactions (e.g., high-valent metal-oxo species versus metal-OOR adducts depending on the ^{18}O-incorporation from $H_2{}^{18}O$ into oxygenated products) (see Scheme 6).[29] Therefore, ^{18}O-labeled water experiments were performed in the styrene epoxidation and cumene hydroxylation by **1**, to understand the nature of the reactive species responsible for the oxygenation reactions by the nonheme iron(III)-acylperoxo complexes (e.g., iron(III)-acylperoxo versus high-valent iron-oxo species). In the ^{18}O-labeled water experiments, no ^{18}O-incorporation from $H_2{}^{18}O$ into the epoxide and alcohol products was observed under any circumstances (Scheme 6B; Experimental Section and SI, Figures S15 and S17), demonstrating that the active oxidant(s) responsible for the olefin epoxidation and alkane hydroxylation reactions by the iron(III)-acylperoxo complex does not exchange its oxygen atom with $H_2{}^{18}O$. Thus, as we have proposed in the olefin epoxidation by chiral iron(III)-acylperoxo complexes (vide supra), the present result supports that the iron(III)-acylperoxo species, not the iron-oxo species formed via the O−O bond cleavage, is the active oxidant that effects the oxygenation reactions (Scheme 6A, $k_1 \gg k_{O-O}$).[30,31]

Scheme 6. Proposed Mechanisms and Reactions for ^{18}O-Labeled Water ($H_2{}^{18}O$) Experiments

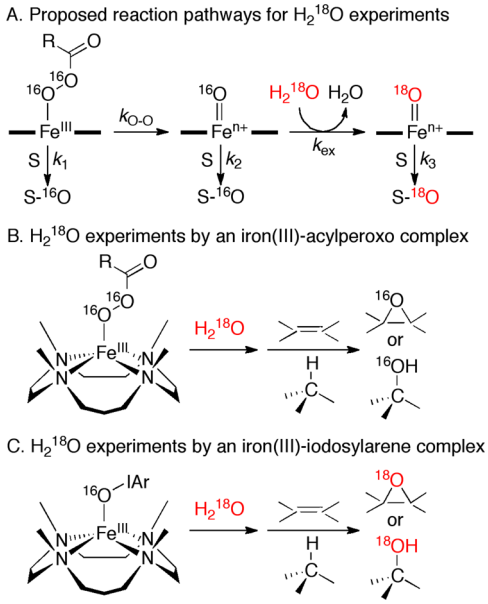

Finally, it is of interest to note that nonheme high-spin iron(III)-iodosylarenes bearing the same supporting ligand, $[(13\text{-TMC})Fe^{III}{-}OIAr]^{3+}$, exchange their atom with labeled water immediately upon addition of $H_2{}^{18}O$ and oxygenate organic substrates with full ^{18}O-incorporation from $H_2{}^{18}O$ into products (Scheme 6C).[13] Thus, by comparing the dramatically different results of the ^{18}O-labeled water experiments obtained in the oxygenation reactions by the iron(III)-acylperoxo and iron(III)-iodosylarene complexes (Schemes 6B and 6C), we propose that the active oxidants are iron(III)-acylperoxo and iron(III)-iodosylarene complexes, not their high-valent iron-oxo counterparts.

CONCLUSIONS

The nature of reactive intermediates in catalytic oxygenation reactions by metalloenzymes and metal complexes has been the subject of much debate over several decades. One way to identify such highly reactive intermediates is to synthesize biomimetic compounds of the intermediates and then use them directly in reactivity studies. Since one of the often-discussed metal-oxygen intermediates in oxygenation reactions is a metal-acylperoxo species, we synthesized mononuclear nonheme high-spin iron(III)-acylperoxo complexes bearing an N-methylated cyclam ligand and characterized them spectroscopically. We then investigated their reactivities in oxygenation reactions, such as olefin epoxidation and alkane hydroxylation. The nonheme high-spin iron(III)-acylperoxo complexes showed high reactivities in the olefin epoxidation and alkane hydroxylation reactions, with high stereo-, chemo-, and enantioselectivities in olefin epoxidation and with high regio- and stereoselectivities in alkane hydroxylation. Moreover, we found that the reactivities of the iron(III)-acylperoxo complexes are very different from those of synthetic nonheme iron(IV)-oxo complexes in both olefin epoxidation and alkane hydroxylation reactions, such as the oxidation of cyclohexene in olefin epoxidation (Scheme 3C) and the $^{18}O_2$ experiment in alkane hydroxylation (Scheme 5A). In addition, based on the results of mechanistic studies, such as the olefin epoxidation by chiral iron(III)-acylperoxo complexes (Scheme 4) and the ^{18}O-labeled water experiments in both olefin epoxidation and alkane hydroxylation reactions (Scheme 6), it became clear that the iron(III)-acylperoxo complexes are strong oxidants capable of oxygenating hydrocarbons prior to their conversion into high-valent iron-oxo species via O−O bond cleavage. In addition, experimental evidence supporting equilibrium between an iron(III)-acylperoxo complex and its corresponding iron(V)-oxo complex and a carboxylic acid (Scheme 7A) was not observed in the present study. Thus, these results are different from the recently reported important study by Münck, Que, Company, Costas, and their co-workers, in which a low-spin iron(III)-acylperoxo complex, $Fe^{III}(OOAc)$, and a high-valent iron(V)-oxo complex, $Fe^{V}(O)(OAc)$, are in equilibrium (Scheme 7B), and the iron(V)-oxo species, not the low-spin iron(III)-acylperoxo complex, is the active oxidant for stereoselective alkane hydroxylation reactions.[16a] Then, the question arises: What causes the different reactivities and mechanisms shown by the high- and low-spin iron(III)-acylperoxo complexes in Scheme 7? We hypothesize that the spin states of iron(III)-acylperoxo complexes (e.g., high- and low-spin iron(III)-acylperoxo complexes) and/or the structures of iron(III)-acylperoxo complexes (e.g., the availability of *cis*-sites for the binding of acylperoxo ligand) are key factors that control reactivities of the nonheme iron(III)-acylperoxo

DOI: 10.1021/jacs.5b13500
J. Am. Chem. Soc. 2016, 138, 2426−2436

Scheme 7. Reactivity Differences between High- and Low-Spin Iron(III)-Acylperoxo Complexes

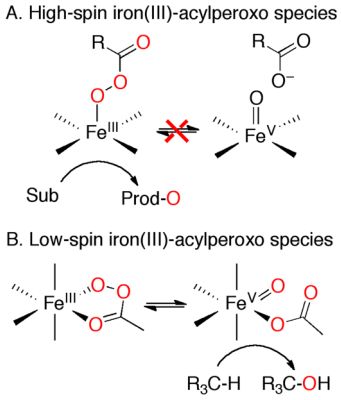

complexes. Thus, future studies will be focused on elucidating the intriguing reactivity differences between high- and low-spin Fe(III)-acylperoxo complexes. This type of reactivity difference has been demonstrated recently in the reactions of high- and low-spin iron(III)-hydroperoxo complexes.[10,11]

EXPERIMENTAL SECTION

Materials. $[Fe^{II}(13\text{-TMC})(CF_3SO_3)_2]$ was prepared according to the literature procedure.[19] $H_2{}^{18}O$ (97% ^{18}O-enriched) and $^{18}O_2$ (98% ^{18}O-enriched) were purchased from ICON Services, Inc. (Summit, NJ, USA). *m*-Chloroperoxybenzoic acid (*m*-CPBA, 77%) and peracetic acid (PAA, 32 wt %) were purchased from Aldrich Chemical Co. Other peroxycarboxylic acids, such as phenylperoxyacetic acid (PPAA), peroxybenzoic acid (PBA), (*R*)-2-phenylperoxypropionic acid, and (*S*)-2-phenylperoxypropionic acid, were prepared as described in the literature.[25,32] All the peroxyacids except peroxyacetic acid were purified by washing with phosphate buffer (pH 7.2) and recrystallized from hexane/ether to remove free carboxylic acid. The purity of the peroxycarboxylic acids was determined by iodometric titration. Peroxycarboxylic acid, once isolated, is stable over long periods of time when stored at 0 °C in a plastic container. All other chemicals were obtained from Aldrich Chemical Co. and used without further purification unless otherwise indicated. Solvents were dried according to the reported procedures and distilled under Ar prior to use.[33] All reactions were performed under an Ar atmosphere or standard Schlenk techniques unless otherwise noted.

Instrumentation. UV–vis spectra were recorded on a Hewlett-Packard Agilent 8453 UV–vis spectrophotometer equipped with a circulating water bath or an UNISOKU cryostat system (USP-203, Japan). ESI-MS were collected on a Thermo Finnigan (San Jose, CA, USA) LCQ Advantage MAX quadrupole ion trap instrument, by infusing samples directly into the source at 20 μL/min using a syringe pump. The spray voltage was set at 4.7 kV and the capillary temperature at 80 °C. EPR spectra were recorded at 5 K using X-band Bruker EMX-plus spectrometer equipped with a dual mode cavity (ER 4116DM). The low temperatures were achieved and controlled with Oxford Instruments ESR900 liquid He quartz cryostat with Oxford Instruments ITC503 temperature and gas flow controller. The experimental parameters for EPR measurements were as follows: microwave frequency = 9.646 GHz, microwave power = 1.0 mW, modulation amplitude = 10 G, gain = 1×10^4, modulation frequency = 100 kHz, time constant = 40.96 ms, and conversion time = 85.00 ms. Mössbauer spectra were recorded at 5 K on a low-field Mössbauer spectrometer equipped with a Janis CCR 5 K cryostat or at 4.2 K on a strong-field Mössbauer spectrometer equipped with an Oxford Instruments Spectromag 4000 cryostat containing an 8 T split-pair superconducting magnet. Both spectrometers were operated in a constant acceleration mode in transmission geometry. The isomer shifts were referenced against that of a metallic iron foil at room temperature. Analysis of the data was performed with the program WMOSS (WMOSS4Mössbauer Spectral Analysis Software, www.wmosss.org, 2009–2015). Product analysis was performed with an Agilent Technologies 6890N gas chromatograph (GC) (HP-5 column, 30 m × 0.32 mm × 0.25 μm film thickness) with a flame ionization detector and Thermo Finnigan (Austin, Texas, USA) FOCUS DSQ (dual stage quadrupole) mass spectrometer interfaced with Finnigan FOCUS gas chromatograph (GC-MS). Free carboxylic acid was quantified by GC equipped with Agilent J&W HP-FFAP column (25 m length × 0.32 mm i.d.; 0.50 μm film thickness). Chromatographic analysis of enantiomers was performed on high-performance liquid chromatography (HPLC, DIOMEX Pump Series P580) equipped with a variable wavelength UV-200 detector and Diacel OD-H column (4.6 mm × 25 cm).

X-ray Absorption Spectroscopy. The Fe K-edge X-ray absorption spectra of $[Fe^{II}(13\text{-TMC})(CF_3SO_3)_2]$, **1**, and $[(13\text{-TMC})Fe^{IV}(O)]^{2+}$ were measured at the Stanford Synchrotron Radiation Lightsource (SSRL) on the unfocused 20-pole 2 T wiggler side-station beamline 7-3 under standard ring conditions of 3 GeV and ~500 mA. A Si(220) double crystal monochromator was used for energy selection. A Rh-coated harmonic rejection mirror was used on beamline 7-3 to reject components of higher harmonics. All complexes were measured as solutions, which were transferred into 2 mm delrin XAS cells with 70 μm Kapton tape windows under synthesis conditions and were immediately frozen after preparation and stored under liquid N_2. During data collection, samples were maintained at a constant temperature of ~10–15 K using an Oxford Instruments CF 1208 liquid helium cryostat. Data were measured to k = 14 $Å^{-1}$ (fluorescence mode) using a Canberra Ge 30-element array detector. Internal energy calibration was accomplished by simultaneous measurement of the absorption of an Fe-foil placed between two ionization chambers situated after the sample. The first inflection point of the foil spectrum was fixed at 7111.2 eV. The samples were monitored for photoreduction, and a small shift in the rising edge energy position was observed over successive scans, indicating X-ray dose related photoreduction of the Fe center. To alleviate this problem, a single scan was obtained from each fresh sample position. For the measurement of $[(13\text{-TMC})Fe^{IV}(O)]^{2+}$, the monochromator was further detuned by 50%. EXAFS data presented here are a 12-scan average for **1**. XANES data presented for $[Fe^{II}(13\text{-TMC})(CF_3SO_3)_2]$, **1**, and $[(13\text{-TMC})Fe^{IV}(O)]^{2+}$ were 7-, 12-, and 8-scan averages, respectively. Data were processed by fitting a second-order polynomial to the pre-edge region and subtracting this from the entire spectrum as background. A four-region spline of orders 2, 3, 3, and 3 was used to model the smoothly decaying postedge region. The data were normalized by subtracting the cubic spline and assigning the edge jump to 1.0 at 7150 eV using the Pyspline program.[34] Data were then renormalized in Kaleidagraph for comparison and quantification purposes.

Theoretical EXAFS signals $\chi(k)$ were calculated by using FEFF (Macintosh version 7.0).[35] Starting structural models were obtained from DFT-optimized structures **1**. The input structure was improved based on preliminary EXAFS fit parameters to generate more accurate theoretical EXAFS signals. Data fitting was performed in EXAFSPAK.[36] The structural parameters that varied during the fitting process were the bond distance (R) and the bond variance σ^2, which is related to the Debye–Waller factor resulting from thermal motion, and static disorder of the absorbing and scattering atoms. The nonstructural parameter ΔE_0 (E_0 = the energy at which k is 0) was also allowed to vary but was restricted to a common value for every component in a given fit. Coordination numbers were systematically varied in the course of the fit but were fixed within a given fit. The coordination number for the short Fe–O distance and the longer Fe–O distances were set to 0.5. Fits accommodating a 40/60 or 60/40 mixture of **1** and $[(13\text{-TMC})Fe^{IV}(O)]^{2+}$ gave poorer fits. However, the accuracy of EXAFS data is not high enough to differentiate between a 50/50, 40/60, and 60/40 mixture of the two forms.

Generation and Characterization of 1–6. The blue intermediates, $[(13\text{-TMC})Fe^{III}(OOC(O)CH_2Ph)]^{2+}$ (**1**), $[(13\text{-TMC})Fe^{III}(OOC(O)Ph)]^{2+}$ (**2**), $[(13\text{-TMC})Fe^{III}(OOC(O)C_6H_4Cl)]^{2+}$ (**3**), $[(13\text{-TMC})Fe^{III}(OOC(O)CH_3)]^{2+}$ (**4**), $[(13\text{-TMC})Fe^{III}(OOC$-

DOI: 10.1021/jacs.5b13500
J. Am. Chem. Soc. 2016, 138, 2426–2436

$(O)^{R}CH(CH_3)Ph)]^{2+}$ (**5**), and $[(13\text{-TMC})Fe^{III}(OOC(O)^{S}CH(CH_3)\text{-}Ph)]^{2+}$ (**6**), were generated by reacting $[Fe^{II}(13\text{-TMC})(CF_3SO_3)_2]$ (1.0 mM) with 4 equiv of PPAA, PBA, *m*-CPBA, PAA, (*R*)-2-phenylperoxypropionic acid, and (*S*)-2-phenylperoxypropionic acid, respectively, in CF_3CH_2OH/acetone (3:1) at −40 °C. The full formation of **1**−**6** was confirmed by monitoring UV−vis spectral changes at 660 nm.

Kinetic Measurements. All reactions were run in a 1.0 cm UV quartz cuvette and followed by monitoring UV−vis spectral changes of the reaction solutions in CF_3CH_2OH/acetone (3:1). Rate constants were determined under pseudo-first-order reaction conditions (e.g., [substrate]/[**1**] > 10) by fitting the absorbance changes at 660 nm for the disappearances of **1**−**4**. In olefin epoxidation, the reactions of **1**−**4** with stilbenes, styrene derivatives, and cyclohexene were investigated at −60 °C. The KIE values for the oxidation reactions of styrene and cyclohexene by **1**−**4** were obtained by using the k_2 values of styrene-h_8/styrene-d_8 and cyclohexene-h_{10}/cyclohexene-d_{10}, respectively. The C−H bond activation reactions by **1** were performed at −40 °C with substrates, such as triphenylmethane (81.0 kcal mol^{-1}), cumene (84.8 kcal mol^{-1}), ethylbenzene (87.0 kcal mol^{-1}), cyclooctane (95.7 kcal mol^{-1}), and cyclohexane (99.5 kcal mol^{-1}).[26] The KIE values for the reaction of **1**−**4** with cumene were determined by comparing k_2 values obtained in the C−H and C−D bond activation reactions of cumene-h_{12} and cumene-d_{12}, respectively. The kinetic experiments were run at least in triplicate, and the data reported represent the average of these reactions.

Product Analysis. Products formed in the reactions of **1** with styrene derivatives, cyclohexene, triphenylmethane, cumene, ethylbenzene, cyclooctane, cyclohexane, adamantane, and *cis*-1,2-dimethylcyclohexane were identified by GC and GC-MS by comparison of the mass peaks and retention time of the products with respect to authentic samples, and the product yields were determined by comparing the responsive peak areas of sample products against standard curves prepared with known authentic compounds using internal standard decane or dodecane. For *cis*- and *trans*-stilbenes, product yields were determined by HPLC equipped with SunFire C18 5 μm column (4.6 mm × 25 cm). The iron products obtained in the reaction of **1** with substrates were analyzed with X-band EPR and ESI-MS spectroscopies.

For the analysis of the O−O bond cleavage product(s) of PPAA, **1** (1.0 mM) was freshly prepared in a solvent mixture of CF_3CH_2OH/acetone (3:1) at −60 °C under an Ar atmosphere, followed by adding styrene (20 mM) to the reaction solution. The reaction mixture was stirred for 10 min at −60 °C, and then PPh_3 (4 mM) was added to quench the reaction. Nitrobenzene was added as an internal standard, and the resulting solution was analyzed directly by GC (Agilent J&W HP-FFAP column) and GC-MS. Product yields were determined by comparing the responsive peak areas of sample products against standard curves prepared with known authentic compounds.

Stoichiometric and Catalytic Asymmetric Epoxidation Reactions. Chalcone (2.0 × 10^2 mM) was added to a solution containing the chiral iron(III)-acylperoxo complexes, **5** or **6**, which was freshly prepared by adding 4 equiv of (*R*)-2-phenylperoxypropionic acid (8.0 mM) or (*S*)-2-phenylperoxypropionic acid (8.0 mM) to a solution of $[Fe^{II}(13\text{-TMC})(CF_3SO_3)_2]$ (2.0 mM) in CF_3CH_2OH/acetone (3:1) at −60 °C. The resulting solution was stirred for 15 min, and then saturated sodium thiosulfate solution was added to quench the reaction. The organic layer was separated and purified through flash column chromatography on silica gel, and the epoxide product was identified by comparison to the HPLC retention time of racemic epoxide. The enantiomeric excess values were determined by HPLC equipped with Diacel OD-H column, and the absolute configuration of the products was determined by comparison with literature reports.

For catalytic epoxidation reactions, (*R*)-2-phenylperoxypropionic acid (40 mM) or (*S*)-2-phenylperoxypropionic acid (40 mM) was added to a solution containing $[Fe^{II}(13\text{-TMC})(CF_3SO_3)_2]$ (2.0 mM) and chalcone (2.0 × 10^2 mM) in CF_3CH_2OH/acetone (3:1) at −60 °C. The resulting solution was stirred for 15 min and then analyzed as described above. There were no oxygenated products when control experiments were carried out in the absence of the iron(II) complex under the identical reaction conditions.

Isotopically Labeled $^{18}O_2$ and $H_2{}^{18}O$ Experiments. For $^{18}O_2$ experiment, both the catalyst and substrates were degassed by four freeze−vacuum−thaw cycles prior to the reaction being performed under an $^{18}O_2$ atmosphere. Cumene (50 mM) was added to a freshly prepared solution of **1** (1.0 mM) in CF_3CH_2OH/acetone (3:1) at −40 °C under $^{18}O_2$ atmosphere. The resulting solution was stirred for 10 min at −40 °C and then directly analyzed by GC-MS. The percentage of ^{18}O in 2-phenylpropan-2-ol was determined by comparison of the relative abundances at m/z = 123 for 2-phenylpropan-2-ol−^{18}O and at m/z = 121 for 2-phenylpropan-2-ol−^{16}O.

For $H_2{}^{18}O$ experiments, $H_2{}^{18}O$ (20 μL, 97% ^{18}O-enriched) and styrene (50 mM) were added to a freshly prepared solution of **1** (1.0 mM) in CF_3CH_2OH/acetone (3:1) under an Ar atmosphere. The resulting solution was stirred for 10 min at −60 °C and then directly analyzed by GC-MS. The percentage of ^{18}O in styrene oxide was determined by comparison of the relative abundances at m/z = 121 for styrene oxide−^{18}O and at m/z = 119 for styrene oxide−^{16}O. Similarly, the $H_2{}^{18}O$ experiment was performed with cumene, and the percentage of ^{18}O in 2-phenylpropan-2-ol was determined as described above for the $^{18}O_2$ experiment.

■ ASSOCIATED CONTENT

Supporting Information

The Supporting Information is available free of charge on the ACS Publications website at DOI: 10.1021/jacs.5b13500.

Tables S1−S9 and Figures S1−S17 (PDF)

■ AUTHOR INFORMATION

Corresponding Authors

*ritis@slac.stanford.edu

*jean-marc.latour@cea.fr

*wwnam@ewha.ac.kr

Notes

The authors declare no competing financial interest.

■ ACKNOWLEDGMENTS

The authors acknowledge the NRF of Korea through CRI (NRF-2012R1A3A2048842 to W.N.) and GRL (NRF-2010-00353 to W.N.). The SSRL SMB Resource is supported primarily by the NIH National Institute of General Medical Sciences (NIGMS) through a Biomedical Technology Research Resource P41 grant (P41GM103393) and contract funds and by the DOE Office of Biological and Environmental Research. J.M.L. acknowledges the support, in part, of Labex ARCANE (ANR-11-LABX-0003-01).

■ REFERENCES

(1) (a) Nam, W. *Acc. Chem. Res.* **2007**, *40*, 465. and review articles in the special issue. (b) Holm, R. H.; Solomon, E. I. *Chem. Rev.* **2014**, *114*, 3367. and review articles in the special issue. (c) Que, L., Jr.; Tolman, W. B. *Nature* **2008**, *455*, 333. (d) Ray, K.; Pfaff, F. F.; Wang, B.; Nam, W. *J. Am. Chem. Soc.* **2014**, *136*, 13942. (e) Chen, Z.; Yin, G. *Chem. Soc. Rev.* **2015**, *44*, 1083. (f) Nam, W. *Acc. Chem. Res.* **2015**, *48*, 2415.

(2) (a) Ortiz de Montellano, P. R. *Cytochrome P450: Structure, Mechanism, and Biochemistry*, 3rd ed.; Springer: Berlin, 2005. (b) Nam, W. *Acc. Chem. Res.* **2007**, *40*, 522. (c) Shaik, S.; Hirao, H.; Kumar, D. *Acc. Chem. Res.* **2007**, *40*, 532. (d) Ortiz de Montellano, P. R. *Chem. Rev.* **2010**, *110*, 932. (e) Costas, M. *Coord. Chem. Rev.* **2011**, *255*, 2912. (f) Krest, C. M.; Onderko, E. L.; Yosca, T. H.; Calixto, J. C.; Karp, R. F.; Livada, J.; Rittle, J.; Green, M. T. *J. Biol. Chem.* **2013**, *288*, 17074.

(3) (a) Abu-Omar, M. M.; Loaiza, A.; Hontzeas, N. *Chem. Rev.* **2005**, *105*, 2227. (b) Krebs, C.; Fujimori, D. G.; Walsh, C. T.; Bollinger, J.

DOI: 10.1021/jacs.5b13500
J. Am. Chem. Soc. 2016, 138, 2426−2436

M., Jr. *Acc. Chem. Res.* **2007**, *40*, 484. (c) Hohenberger, J.; Ray, K.; Meyer, K. *Nat. Commun.* **2012**, *3*, 720. (d) Solomon, E. I.; Light, K. M.; Liu, L. V.; Srnec, M.; Wong, S. D. *Acc. Chem. Res.* **2013**, *46*, 2725. (e) Nam, W.; Lee, Y.-M.; Fukuzumi, S. *Acc. Chem. Res.* **2014**, *47*, 1146. (f) Cook, S. A.; Borovik, A. S. *Acc. Chem. Res.* **2015**, *48*, 2407.

(4) Rittle, J.; Green, M. T. *Science* **2010**, *330*, 933.

(5) (a) Gunay, A.; Theopold, K. H. *Chem. Rev.* **2010**, *110*, 1060. (b) Borovik, A. S. *Chem. Soc. Rev.* **2011**, *40*, 1870. (c) De Visser, S. P.; Rohde, J.-U.; Lee, Y.-M.; Cho, J.; Nam, W. *Coord. Chem. Rev.* **2013**, *257*, 381. (d) Fukuzumi, S. *Coord. Chem. Rev.* **2013**, *257*, 1564. (e) Cho, K.-B.; Hajime, H.; Shaik, S.; Nam, W. *Chem. Soc. Rev.* **2016**, DOI: 10.1039/C5CS00566C. (f) Puri, M.; Que, L., Jr. *Acc. Chem. Res.* **2015**, *48*, 2443.

(6) (a) Price, J. C.; Barr, E. W.; Tirupati, B.; Bollinger, J. M., Jr.; Krebs, C. *Biochemistry* **2003**, *42*, 7497. (b) Rohde, J.-U.; In, J.-H.; Lim, M. H.; Brennessel, W. W.; Bukowski, M. R.; Stubna, A.; Münck, E.; Nam, W.; Que, L., Jr. *Science* **2003**, *299*, 1037.

(7) (a) Newcomb, M.; Hollenberg, P. F.; Coon, M. J. *Arch. Biochem. Biophys.* **2003**, *409*, 72. (b) Newcomb, M.; Toy, P. H. *Acc. Chem. Res.* **2000**, *33*, 449. (c) Vaz, A. D. N.; McGinnity, D. F.; Coon, M. J. *Proc. Natl. Acad. Sci. U. S. A.* **1998**, *95*, 3555. (d) Volz, T. J.; Rock, D. A.; Jones, J. P. *J. Am. Chem. Soc.* **2002**, *124*, 9724. (e) Cryle, M. J.; De Voss, J. J. *Angew. Chem., Int. Ed.* **2006**, *45*, 8221.

(8) (a) Shaik, S.; Hirao, H.; Kumar, D. *Nat. Prod. Rep.* **2007**, *24*, 533. (b) Song, W. J.; Ryu, Y. O.; Song, R.; Nam, W. *JBIC, J. Biol. Inorg. Chem.* **2005**, *10*, 294. (c) Nam, W.; Ryu, Y. O.; Song, W. J. *JBIC, J. Biol. Inorg. Chem.* **2004**, *9*, 654. (d) Shaik, S.; de Visser, S. P.; Kumar, D. *JBIC, J. Biol. Inorg. Chem.* **2004**, *9*, 661.

(9) Solomon, E. I.; Wong, S. D.; Liu, L. V.; Decker, A.; Chow, M. S. *Curr. Opin. Chem. Biol.* **2009**, *13*, 99.

(10) Cho, J.; Jeon, S.; Wilson, S. A.; Liu, L. V.; Kang, E. A.; Braymer, J. J.; Lim, M. H.; Hedman, B.; Hodgson, K. O.; Valentine, J. S.; Solomon, E. I.; Nam, W. *Nature* **2011**, *478*, 502.

(11) (a) Park, M. J.; Lee, J.; Suh, Y.; Kim, J.; Nam, W. *J. Am. Chem. Soc.* **2006**, *128*, 2630. (b) Liu, L. V.; Hong, S.; Cho, J.; Nam, W.; Solomon, E. I. *J. Am. Chem. Soc.* **2013**, *135*, 3286. (c) Kim, Y. M.; Cho, K.-B.; Cho, J.; Wang, B.; Li, C.; Shaik, S.; Nam, W. *J. Am. Chem. Soc.* **2013**, *135*, 8838.

(12) (a) Draksharapu, A.; Angelone, D.; Quesne, M. G.; Padamati, S. K.; Gómez, L.; Hage, R.; Costas, M.; Browne, W. R.; de Visser, S. P. *Angew. Chem., Int. Ed.* **2015**, *54*, 4357. (b) Wang, C.; Kurahashi, T.; Fujii, H. *Angew. Chem., Int. Ed.* **2012**, *51*, 7809. (c) Cong, Z.; Yanagisawa, S.; Kurahashi, T.; Ogura, T.; Nakashima, S.; Fujii, H. *J. Am. Chem. Soc.* **2012**, *134*, 20617. (d) Lennartson, A.; McKenzie, C. J. *Angew. Chem., Int. Ed.* **2012**, *51*, 6767. (e) Guo, M.; Dong, H.; Li, J.; Cheng, B.; Huang, Y.-q.; Feng, Y.-q.; Lei, A. *Nat. Commun.* **2012**, *3*, 1190.

(13) (a) Hong, S.; Wang, B.; Seo, M. S.; Lee, Y.-M.; Kim, M. J.; Kim, H. R.; Ogura, T.; Carcia-Serres, R.; Clémancey, M.; Latour, J.-M.; Nam, W. *Angew. Chem., Int. Ed.* **2014**, *53*, 6388. (b) Wang, B.; Lee, Y.-M.; Seo, M. S.; Nam, W. *Angew. Chem., Int. Ed.* **2015**, *54*, 11740.

(14) (a) Makhlynets, O. V.; Oloo, W. N.; Moroz, Y. S.; Belaya, I. G.; Palluccio, T. D.; Filatov, A. S.; Müller, P.; Cranswick, M. A.; Que, L., Jr.; Rybak-Akimova, E. V. *Chem. Commun.* **2014**, *50*, 645. (b) Oloo, W. N.; Meier, K. K.; Wang, Y.; Shaik, S.; Münck, E.; Que, L., Jr. *Nat. Commun.* **2014**, *5*, 3046. (c) Nakazawa, J.; Terada, S.; Yamada, M.; Hikichi, S. *J. Am. Chem. Soc.* **2013**, *135*, 6010. (d) Hikichi, S.; Hanaue, K.; Fujimura, T.; Okuda, H.; Nakazawa, J.; Ohzu, Y.; Kobayashi, C.; Akita, M. *Dalton Trans.* **2013**, *42*, 3346. (e) Zhang, X.; Furutachi, H.; Tojo, T.; Tsugawa, T.; Fujinami, S.; Sakurai, T.; Suzuki, M. *Chem. Lett.* **2011**, *40*, 515. (f) Hessenauer-Ilicheva, N.; Franke, A.; Meyer, D.; Woggon, W.-D.; van Eldik, R. *J. Am. Chem. Soc.* **2007**, *129*, 12473. (g) Soper, J. D.; Kryatov, S. V.; Rybak-Akimova, E. V.; Nocera, D. G. *J. Am. Chem. Soc.* **2007**, *129*, 5069. (h) Machii, K.; Watanabe, Y.; Morishima, I. *J. Am. Chem. Soc.* **1995**, *117*, 6691. (i) Kitajima, N.; Fujisawa, K.; Moro-oka, Y. *Inorg. Chem.* **1990**, *29*, 357. (j) Groves, J. T.; Watanabe, Y. *Inorg. Chem.* **1987**, *26*, 785. (k) Ghosh, P.; Tyeklar, Z.; Karlin, K. D.; Jacobson, R. R.; Zubieta, J. *J. Am. Chem. Soc.* **1987**, *109*, 6889. (l) Groves, J. T.; Watanabe, Y.; McMurry, T. J. *J. Am. Chem. Soc.* **1983**, *105*, 4489. (m) Kikunaga, T.; Matsumoto, T.; Ohta, T.; Nakai, H.; Naruta, Y.; Ahn, K.-H.; Watanabe, Y.; Ogo, S. *Chem. Commun.* **2013**, *49*, 8356.

(15) MacBeth, C. E.; Gupta, R.; Mitchell-Koch, K. R.; Young, V. G.; Lushington, G. H.; Thompson, W. H.; Hendrich, M. P.; Borovik, A. S. *J. Am. Chem. Soc.* **2004**, *126*, 2556.

(16) (a) Serrano-Plana, J.; Oloo, W. N.; Acosta-Rueda, L.; Meier, K. K.; Verdejo, B.; García-España, E.; Basallote, M. G.; Münck, E.; Que, L., Jr.; Company, A.; Costas, M. *J. Am. Chem. Soc.* **2015**, *137*, 15833. (b) Lyakin, O. Y.; Zima, A. M.; Samsonenko, D. G.; Bryliakov, K. P.; Talsi, E. P. *ACS Catal.* **2015**, *5*, 2702. (c) Panda, C.; Debgupta, J.; Díaz, D. D.; Singh, K. K.; Gupta, S. S.; Dhar, B. B. *J. Am. Chem. Soc.* **2014**, *136*, 12273. (d) Ghosh, M.; Singh, K. K.; Panda, C.; Weitz, A.; Hendrich, M. P.; Collins, T. J.; Dhar, B. B.; Gupta, S. S. *J. Am. Chem. Soc.* **2014**, *136*, 9524. (e) Van Heuvelen, K. M.; Fiedler, A. T.; Shan, X.; De Hont, R. F.; Meier, K. K.; Bominaar, E. L.; Münck, E.; Que, L., Jr. *Proc. Natl. Acad. Sci. U. S. A.* **2012**, *109*, 11933. (f) Lyakin, O. Y.; Bryliakov, K. P.; Britovsek, G. J. P.; Talsi, E. P. *J. Am. Chem. Soc.* **2009**, *131*, 10798. (g) de Oliveira, F. T.; Chanda, A.; Banerjee, D.; Shan, X.; Mondal, S.; Que, L., Jr.; Bominaar, E. L.; Münck, E.; Collins, T. J. *Science* **2007**, *315*, 835.

(17) McDonald, A. R.; Que, L., Jr. *Coord. Chem. Rev.* **2013**, *257*, 414.

(18) Gütlich, P.; Bill, E.; Trautwein, A. X. *Mössbauer Spectroscopy and Transition Metal Chemistry: Fundamentals and Applications*; Springer-Verlag: Berlin Heidelberg, 2011; Chapter 4, pp 73−135.

(19) Hong, S.; So, H.; Yoon, H.; Cho, K.-B.; Lee, Y.-M.; Fukuzumi, S.; Nam, W. *Dalton trans.* **2013**, *42*, 7842.

(20) (a) Ostovic, D.; Bruice, T. C. *Acc. Chem. Res.* **1992**, *25*, 314. (b) Traylor, T. G.; Xu, F. *J. Am. Chem. Soc.* **1988**, *110*, 1953.

(21) (a) Annaraj, J.; Kim, S.; Seo, M. S.; Lee, Y.-M.; Kim, Y.; Kim, S.-J.; Choi, Y. S.; Jang, H. G.; Nam, W. *Inorg. Chim. Acta* **2009**, *362*, 1031. (b) Singh, K. K.; Tiwari, M. K.; Dhar, B. B.; Vanka, K.; Gupta, S. S. *Inorg. Chem.* **2015**, *54*, 6112.

(22) (a) Groves, J. T.; Watanabe, Y. *Inorg. Chem.* **1986**, *25*, 4808. (b) Higuchi, T.; Shimada, K.; Maruyama, N.; Hirobe, M. *J. Am. Chem. Soc.* **1993**, *115*, 7551. (c) Suzuki, N.; Higuchi, T.; Nagano, T. *J. Am. Chem. Soc.* **2002**, *124*, 9622. (d) Miyazaki, Y.; Satake, A.; Kobuke, Y. *J. Mol. Catal. A: Chem.* **2008**, *283*, 129. (e) Song, Y. J.; Hyun, M. Y.; Lee, J. H.; Lee, H. G.; Kim, J. H.; Jang, S. P.; Noh, J. Y.; Kim, Y.; Kim, S.-J.; Lee, S. J.; Kim, C. *Chem. - Eur. J.* **2012**, *18*, 6094. (f) Hyun, M. Y.; Jo, Y. D.; Lee, J. H.; Lee, H. G.; Park, H. M.; Hwang, I. H.; Kim, K. B.; Lee, S. J.; Kim, C. *Chem. - Eur. J.* **2013**, *19*, 1810.

(23) (a) Dhuri, S. N.; Cho, K.-B.; Lee, Y.-M.; Shin, S. Y.; Kim, J. H.; Mandal, D.; Shaik, S.; Nam, W. *J. Am. Chem. Soc.* **2015**, *137*, 8623. (b) Kwon, Y. H.; Mai, B. K.; Lee, Y.-M.; Dhuri, S. N.; Mandal, D.; Cho, K.-B.; Kim, Y.; Shaik, S.; Nam, W. *J. Phys. Chem. Lett.* **2015**, *6*, 1472.

(24) Oloo, W. N.; Feng, Y.; Lyer, S.; Parmelee, S.; Xue, G.; Que, L., Jr. *New J. Chem.* **2013**, *37*, 3411.

(25) (a) Collins, J. F.; McKervey, M. A. *J. Org. Chem.* **1969**, *34*, 4172. (b) Silbert, L. S.; Siegel, E.; Swern, D. *J. Org. Chem.* **1962**, *27*, 1336. (c) Folli, U.; Iarossi, D.; Montanari, F.; Torre, G. *J. Chem. Soc. C* **1968**, 1317. (d) Folli, U.; Iarossi, D.; Montanari, F. *J. Chem. Soc. C* **1968**, 1372. (e) Montanari, F.; Moretti, I.; Torre, G. *J. Chem. Soc. D* **1969**, 135.

(26) Luo, Y-R. *Comprehensive Handbook of Chemical Bond Energies*; Taylor & Francis: Boca Raton, FL, 2007.

(27) (a) Groves, J. T.; Nemo, T. E. *J. Am. Chem. Soc.* **1983**, *105*, 6243. (b) Brown, R. B.; Hill, C. L. *J. Org. Chem.* **1988**, *53*, 5762. (c) Barton, D. H. R.; Beck, A. H.; Taylor, D. K. *Tetrahedron* **1995**, *51*, 5245. (d) Chen, K.; Que, L., Jr. *J. Am. Chem. Soc.* **2001**, *123*, 6327. (e) Mitra, M.; Lloret-Fillol, J.; Haukka, M.; Costas, M.; Nordlander, E. *Chem. Commun.* **2014**, *50*, 1408. (f) Olivo, G.; Nardi, M.; Vìdal, D.; Barbieri, A.; Lapi, A.; Gómez, L.; Lanzalunga, O.; Costas, M.; Stefano, S. D. *Inorg. Chem.* **2015**, *54*, 10141.

(28) (a) Sono, M.; Roach, M. P.; Coulter, E. D.; Dawson, J. H. *Chem. Rev.* **1996**, *96*, 2841. (b) Groves, J. T.; Nemo, T. E.; Myers, R. S. *J. Am. Chem. Soc.* **1979**, *101*, 1032. (c) Kim, C.; Chen, K.; Kim, J.; Que, L., Jr. *J. Am. Chem. Soc.* **1997**, *119*, 5964. (d) Nam, W.; Goh, Y. M.; Lee, Y.

DOI: 10.1021/jacs.5b13500
J. Am. Chem. Soc. 2016, 138, 2426−2436

J.; Lim, M. H.; Kim, C. *Inorg. Chem.* **1999**, *38*, 3238. (e) Gómez, L.; Garcia-Bosch, I.; Company, A.; Benet-Buchholz, J.; Polo, A.; Sala, X.; Ribas, X.; Costas, M. *Angew. Chem., Int. Ed.* **2009**, *48*, 5720. (f) Prat, I.; Company, A.; Postils, V.; Ribas, X.; Que, L., Jr.; Luis, J. M.; Costas, M. *Chem. - Eur. J.* **2013**, *19*, 6724.

(29) (a) Meunier, B.; Bernadou, J. *Top. Catal.* **2002**, *21*, 47. (b) Nam, W.; Kim, I.; Lim, M. H.; Choi, H. J.; Lee, J. S.; Jang, H. G. *Chem. - Eur. J.* **2002**, *8*, 2067. (c) Groves, J. T.; Lee, J.; Marla, S. S. *J. Am. Chem. Soc.* **1997**, *119*, 6269. (d) Lee, K. A.; Nam, W. *J. Am. Chem. Soc.* **1997**, *119*, 1916. (e) Bernadou, J.; Fabiano, A.-S.; Robert, A.; Meunier, B. *J. Am. Chem. Soc.* **1994**, *116*, 9375. (f) Nam, W.; Valentine, J. S. *J. Am. Chem. Soc.* **1993**, *115*, 1772. (g) Groves, J. T.; Haushalter, R. C.; Nakamura, M.; Nemo, T. E.; Evans, B. J. *J. Am. Chem. Soc.* **1981**, *103*, 2884.

(30) We cannot rule out a possibility that although the oxygenating intermediate is an iron-oxo species. The oxygen atoms in the epoxide and alcohol products may not derive from the labeled water if the rate of the oxygen exchange between the iron-oxo species and labeled water is much slower than that of the oxygenation reaction by the iron-oxo species (Scheme 6A, $k_{ex} \ll k_2$). Nonetheless, we expect that an iron(V)-oxo species exchanges its oxygen atom with $H_2{}^{18}O$ at a fast rate.

(31) Unfortunately, no ^{18}O-labeled water experiments were performed in the alkane hydroxylation reactions by a nonheme iron(V)-oxo species: see ref 16a.

(32) (a) McDonald, R. N.; Steppel, R. N.; Dorsey, J. E. *Org. Synth.* **1970**, *50*, 15. (b) Ogata, Y.; Sawaki, Y. *Tetrahedron* **1967**, *23*, 3327.

(33) Armarego, W. L. F.; Chai, C. L. L. *Purification of Laboratory Chemicals*, 6th ed.; Pergamon Press: Oxford, U.K., 2009.

(34) Tenderholt, A.; Hedman, B.; Hodgson, K. O. *AIP Conf. Proc.* **2007**, *882*, 105.

(35) (a) Zabinsky, S. I.; Rehr, J. J.; Ankudinov, A.; Albers, R. C.; Eller, M. J. *Phys. Rev. B: Condens. Matter Mater. Phys.* **1995**, *52*, 2995. (b) Rehr, J. J.; Mustre de Leon, J.; Zabinsky, S. I.; Albers, R. C. *J. Am. Chem. Soc.* **1991**, *113*, 5135. (c) Mustre de Leon, J.; Rehr, J. J.; Zabinsky, S. I.; Albers, R. C. *Phys. Rev. B: Condens. Matter Mater. Phys.* **1991**, *44*, 4146.

(36) George, G. N. *EXAFSPAK and EDG-FIT. Stanford Synchrotron Radiation Laboratory*; Stanford Linear Accelerator Center: Stanford, CA, 2000.

DOI: 10.1021/jacs.5b13500
J. Am. Chem. Soc. 2016, 138, 2426−2436